JOINT EUROPEAN TORUS JET

JET–P(93)81

R. Giannella, L. Lauro-Taroni, M. Mattioli,
B. Alper, B. Denne-Hinnov, G. Magyar, J. O'Rourke, D. Pasini

Role of Current Profile and Heating Power in Impurity Transport in JET L-mode Discharges

Role of Current Profile and Heating Power in Impurity Transport in JET L-mode Discharges

R. Giannella, L. Lauro-Taroni, M. Mattioli[1]
B. Alper, B. Denne-Hinnov, G. Magyar, J. O'Rourke, D. Pasini[2]

JET-Joint Undertaking, Culham Science Centre, OX14 3DB, Abingdon, UK

[1]Association Euratom-CEA sur la Fusion, Cadarache, France.
[2]Commission of the European Communities, Directorate General for Science Research and Development, Brussels, Belgium.

Preprint of a paper to be submitted for publication in
Nuclear Fusion
December 1993

ABSTRACT

Results are presented of transport studies conducted on trace impurities injected with the laser blow-off technique in a variety of L-mode pulses. In the core of the discharge, the transport is much slower, the impurity diffusion coefficient D is more than an order of magnitude below the values it assumes further out, but still above the neoclassical predictions. The extent of the slow transport core region varies with the magnetic field and with the total plasma current and is broadly correlated with the edge value of the safety factor. Closer analysis reveals that the current profile is essential in determining the radial dependence of D. This parameter appears to undergo a rapid transition to highly anomalous levels in the vicinity of the radial position where the dimensionless shear parameter is equal to 0.5. Within that region D stays moderate even when the electron temperature gradient is high. A marked increase of D in the outer region of the discharge is observed when the power per particle is raised or, alternatively when the temperature and its gradient grow in that region, but no clear dependence of D on plasma density is found when the electron temperature profile is kept constant. Transport modelling based on the critical ∇T_e assumption leads to D-profiles that are similar, although not in detailed quantitative agreement, to the experimental ones when the temperature profiles are flat in the centre; when the temperature profiles are peaked in the centre, even the radial dependence of the predicted diffusion profiles is very different fron the one observed. Recent theoretical attempts to analyze the radial structure of the microturbulent fluctuations predict a strong positive dependence of anomalous diffusion on the magnetic shear as observed in our experiments.

1. INTRODUCTION

Much work has been done recently on impurity transport in Tokamaks. The state of the art around 1990 has been reviewed in Ref. [1]. The best diagnosis of the impurity transport has been achieved in laser blow-off injection experiments by following both in space and time the radiation signals (VUV emission line intensities, soft X-rays and bolometric tomographic data) emitted by the injected impurity ions. Well-known advantages of this technique are the control of the injection time and of the amount of the injected material as well as the short duration of the source. The decay times of the brightnesses of either the central ion lines or of the central soft X-rays are sometimes identified with the impurity containment time τ_I and are quite often used to compare different discharge

regimes. For fine studies of the transport, however, it is necessary to use an impurity transport code in which the radial flux density is described as the sum of both diffusive and convective terms (with diffusion coefficient D and inward convective velocity V), whose radial dependencies are obtained by detailed comparison of experimental and simulated data.

In JET, reported laser blow-off studies [2,3,4] have confirmed previous conclusions based on intrinsic emission analysis, namely degradation of confinement with additional power, obtainment of very large τ_I values during H-modes, less than linear dependence of τ_I on the electron density n_e and on the safety factor q for ohmic plasmas. These studies have clearly shown that between sawtooth crashes the transport of impurities is very fast in the outer region but very much slower in the core. The transport is greatly enhanced during sawtooth crashes effectively short-circuiting these two distinct transport regions. For the quiescent phases the radius dependent transport parameters D and V were determined. Each sawtooth crash requires *ad-hoc* treatment for a short time (of the order of one hundred microseconds): the transport parameters are much increased in such a way as to simulate correctly the discontinuity of the soft X-ray emissivity profiles. In cases of monster sawteeth, however, the quiescent phases between sawtooth crashes are considerably longer than τ_I avoiding the need to reproduce the above mentioned discontinuities in the transport simulation.

Similarities between impurity and electron particle transport have been found [5,6] in ohmic plasmas (including pellet-fuelled plasmas). For electrons the diffusion coefficients D were typically one half of those for impurities (in the m^2/s range), whereas the inward electron convection velocities were one order of magnitude smaller than the corresponding velocities for impurities [5,7,8] (respectively, in the tenth of m/s and in the m/s ranges).

These studies however were performed only for a limited class of JET discharges, namely plasma current $I_p \cong 3$ MA and toroidal field $B_T \cong 3.2$ T, and included ohmic, L-mode and H-mode plasmas.

This paper reports on more systematic L-mode studies performed recently in order to analyse the variability of impurity transport depending on operative conditions (e.g. steady state or varying current profile) and operation parameters (n_e, I_p, B_T and additional power P_{add}). Preliminary results have been already presented at the Innsbruck [9] and Lisbon [10] EPS Conferences in 1992 and 1993.

Section 2 contains a description of the experimental conditions and the results obtained. In Section 3, after a short review of the simulation code including the atomic physics involved, numerical simulations are presented for a particular pulse (#27394) having all the operating parameters in the middle of the respective spanned regions. Plots of D(r) and V(r) for different discharges are presented to show their dependence on electron density, plasma current, total (additional plus ohmic) heating power as well as the effect of transient I_p conditions for I_p = 7 MA discharges. The diffusion coefficient outside the central region is subsequently analysed in Section 4 with regard to its dependence on the discharge parameters. The radial extension of the reduced transport region is compared with the size of the q = 1 magnetic surface and the correlation of low diffusivity with low magnetic shear is analysed. In the following Section 5 the reduced diffusivity of the inner plasma region is compared with the predictions of the neoclassical theory. Since the transport parameters in the outer region are much larger than the neo-classical predictions, comparisons with empirical and theoretical (based on microturbulence) models of anomalous transport are also made in the same section. Concluding remarks and a summary of the paper are presented in Section 6.

2. DESCRIPTION OF THE EXPERIMENTS

Although a variety of plasma operation scenarios and confinement modes has been studied at JET in the past with laser blow-off experiments [2,3,4], the toroidal plasma current I_p and the toroidal magnetic field B_T ranges explored, as well as those of the electron density n_e and additional power P_{add}, were very limited. Because of these limitations no significant analysis of the dependence of transport parameters on these variables could be performed. The data acquired during 1992 largely overcome these limitations for L-mode discharges.

The discharges discussed in this paper explore virtually the whole practical ranges of I_p (2 to 7 MA) and B_T (1.45 to 3.4 T) for the JET device. In fig. 1 these discharges are represented by their trajectories in the q_a- ℓ_i plane during a period of 1 sec starting 0.5 sec before impurity injection. Most of the data on the figure refer to discharges where the current profile is in a quasi steady state (indicated by the short length of the trajectories). Nearly all these discharges are affected by frequent sawtooth activity and their electron temperature profiles are rather flat in the central region extending out to the sawtooth inversion surface. The

temperature profiles are, on the other hand, quite peaked in monster sawtooth cases (pulses #18112 and #27739). On the plot a few discharges also appear (#27342, #27878, #27889) where the total plasma current was varying or where the current profile was evolving before the onset of sawteeth. In these discharges the fixed relationship between the value of the safety factor at the plasma edge q_a and the internal inductance ℓ_i, observable for the quasi steady state class of pulses, appears to be broken.

The density $\left(\langle n_e \rangle = 1 \text{ to } 5 \cdot 10^{19} \text{m}^{-3}\right)$ and additional power (P_{add} = 0 to 20 MW) ranges are also quite representative of the operation domain of JET. The additional power is supplied in most cases by ion cyclotron radio-frequency (RF) heating, but some pulses with neutral beam injection (NBI) are also included. The discharges were run in ^{4}He as well as D plasmas. All the discharges were performed in the limiter configuration and they are all in the ohmic or L-mode regime.

The injected impurities include Fe, Ni and Ag. No dependence of the diffusion coefficient D and of the inward convection velocity V on the background gas species (of mass m_{bg} and charge Z_{bg}) or on the injected element was observed in these discharges as was the case for ohmically heated plasmas on TFTR [11]. This result does not contradict the scaling law for τ_I found on Alcator-C ($\tau_I \propto m_{bg}/Z_{bg}$) [12] since the ratio m_{bg}/Z_{bg} is the same for ^{4}He and D.

Out of 1 to $3 \cdot 10^{18}$ atoms reaching the scrape-off layer from the target chamber [13], about one quarter is found in the main plasma resulting in impurity ion densities up to a few 10^{16} m^{-3} at the plasma edge and, although their contribution to the electron density is always very small within the separatrix, the average ion charge can be substantially affected (ΔZ_{eff} = 1 to 2) at the edge during 10 to 20 msec after the injection. The impurity strength parameter $\alpha = n_I Z_I^2 / n_i Z_i^2$ (see e.g. Ref. [14]), measuring the ratio of the collision frequencies ν_{II} and ν_{iI}, is 0.1 or lower, with the mentioned exception of the first few tens of milliseconds at the plasma edge where it is O(1); so over most of the discharge the injected ions propagate as test particles. Here n_I, n_i and Z_I, Z_i are the total densities and average charge numbers of the injected impurity and of the main plasma ions, respectively, and ν_{II}, ν_{iI} are the I-I and i-I collision frequencies.

The perturbation induced by the injection on the global plasma parameters is typically very low $\left(|\Delta I_p| / I_p < 0.2\%,\ \Delta\langle n_e \rangle / \langle n_e \rangle < 1\%,\ |\Delta W| / W < 5\%,\right.$. W being the

plasma energy. Local perturbations on n_e can, however, be significant at the plasma edge. With the outermost vertical channel of the interferometric diagnostic (probing the plasma at $\rho \geq 0.9$) a maximum line integrated density rise of ~ 10 % is measured in low density discharges following injection of nickel (here ρ is the normalised minor radius). This is consistent with the number of electrons lost in the first few centimetres due to ionisation of the injected atoms (e.g. Ni^0 to Ni^{+15}). However in most pulses the amount is not detectable with interferometry, i.e. it is lower than 1 %. The electron temperature generally suffers a reduction not larger than 3 % at the centre and in any case lower than 10 % within $\rho = 0.85$, i.e. over the region normally monitored with good time resolution by the electron cyclotron emission T_e diagnostics. As the duration of these perturbations is typically of the order of 0.2 sec (to be compared with a typical internal resistive time constant of 2 sec or longer) and the perturbation of Z_{eff} in the region mentioned before is 15 % or lower, the modifications induced on the current density j are estimated to be lower than 3 % at the edge of that region and considerably smaller at the centre. These perturbations are comparable to or smaller than the fluctuations on j induced by the sawteeth in JET discharges [15] and much smaller than the experimental uncertainties on the absolute value of j.

The main diagnostics used are VUV [16], XUV [17], and soft X-ray [18] spectrometers recording, along lines of sight aiming at the plasma core, the intensities of emission lines from different charge states (Ni XIII, XVII, XVIII, XX to XXVII, Fe XV, XVIII to XXIV and Ag XVIII, XIX, XXXVI, XXXVII are monitored during the experiments described here). The multi-chord bolometric diagnostic [19] and the tomographic soft X-ray cameras [20] are also utilised.

The latter diagnostic provides space-resolved information on the density of ion populations present in the discharge and contributing to the soft X-ray emission through bremsstrahlung, radiative recombination and line radiation. (With the 250 μm thick Be filter used in the experiments considered here, the latter process is contributing appreciably to the measured signals only for heavy elements starting from Cl.) The soft X-ray emissivity ε_{SXR} can be written as $\varepsilon_{SXR} = \Sigma_\ell n_e n_\ell Q_{SXR\ell}$, where $Q_{SXR\ell}$ is an effective rate coefficient for radiation emission in the range of sensitivity of the soft X-ray cameras; here the sum is extended over all the elements in the discharge, including the background gas. $Q_{SXR\ell}$ depends both on the distribution among different ion states of the element ℓ and on the electron temperature, and is consequently different for plasmas at

corona ionisation equilibrium (CIE) or for either ionising or recombining plasmas. In Ref. [21], from ε_{SXR} the plasma chemical composition (i.e. all the densities n_ℓ and the effective charge Z_{eff}) was deduced assuming CIE.

In this paper we are interested only in the analysis of the injected impurity. However the direct deduction of its radial density profile from the soft X-ray emissivity involves a number of difficulties. Firstly the emissivity due to the injected impurity $\Delta\varepsilon_{SXR}$ is superimposed on a background that is itself not strictly constant in time (due, for example, to the oscillation of the electron temperature T_e in connection with the sawtooth activity). Secondly the limited spatial resolution of the tomographic inversion distorts the gradients of the deduced emissivities.

Finally a crucial difficulty lies in the evaluation of the coefficients Q_{SXRI} for the injected element I. In Ref. [22], based on the analysis already presented in Ref. [21] the density of the injected impurity is computed as $n_I = \Delta\varepsilon_{SXR}/(Q_{SXRI}\cdot n_e)$ assuming CIE temperature dependence for Q_{SXRI}. From $n_I(r,t)$ the radial flux density $\Gamma_I(r,t)$ was then obtained using the continuity equation

$$\partial n_I/\partial t = - 1/r\, \partial(r\Gamma_I)/\partial r.$$

The ansatz that the impurity flow can be described as the sum of a diffusive plus a convective term, $\Gamma_I = - D\, \partial n_I/\partial r - V\, n_I$, was checked by fitting straight lines to the plots of Γ_I/n_I at given values of the minor radius r versus $1/n_I\, \partial n_I/\partial r$ at the same positions. For every r, D(r) is given by the slope of the corresponding straight line and V(r) by its intercept with the Γ_I/n_I axis. This analysis has indicated, for laser blow-off injected Ni, D(r) functions increasing with radius. On the other hand, the straight lines intercept the Γ_I/n_I axis near the origin with large uncertainties implying V(r)-values of the order of 1 m/s or smaller. Simulations with the impurity transport code of the same shots have indicated the correct shape of the D(r) functions deduced with the method of Ref.[22]. However, with the exception of the centre of the discharge (were the errors are too large to make an accurate comparison) the numerical values of D obtained are larger by a factor of 2 to 3 with respect to the simulations. This discrepancy has been again verified for one of the 1992 JET shots (#27415). In fig. 2 Q_{SXR} as given by the simulation at different times is plotted as function of T_e (using the $T_e(r)$ dependence). The thick solid line gives Q_{SXR} at CIE, i.e. the curve used in the analysis of Refs. [21,22]. Clearly at early times the CIE curve gives ε_{SXR} values too large, then the derived

n_I-values are too low. The difference diminishes with time, so that $\partial n_I/\partial t$ and consequently Γ_I are over estimated.

Shot number #27394 is taken as reference shot since all its parameters are in the middle of the scanned ranges. They are I_p = 3 MA, B_T = 3.2 T, $n_e(0) = 3.7 \cdot 10^{19}$, $T_e(0)$ = 4.0 keV, P_{add} = 4 MW, with the parameter $P_{tot}/\langle n_e \rangle \equiv (P_{add}+P_\Omega)/\langle n_e \rangle = 2.1 \cdot 10^{-13}$ Wm^3. Evolution of plasma parameters is shown in fig. 3 (top), whereas on the same figure (bottom) the tomographically inverted soft X-ray emissivity perturbations $\Delta\varepsilon_{SXR}$ along a horizontal radial chord following Ni injection are presented.

The latter shows the most conspicuous feature found in all the pulses investigated in all confinement regimes, that is the slowness of the transport in the centre with respect to the rest of the discharge. Fig. 4 shows this in more detail. During the ingress phase the impurities propagate rapidly inwards untill they reach an intermediate radial position, then their progression is very strongly slowed down. Locally $\Delta\varepsilon_{SXR}$ is seen to increase by a factor of 3 over a period of 30 msec while the peak only moves radially by about 0.1 m and the emission in the plasma core does not increase appreciably. This behaviour is the evidence that across the flux surface through the radial position *a* in fig. 4 (top) the inward impurity flow is comparatively high, because the emissivity $\Delta\varepsilon_{SXR}$ and, therefore, the Ni density $n_I(r)$ increase substantially within that surface. Across the surface *b* the flows are much lower instead, because no substantial increase of Ni ions is detected within that region. Conversely the radial derivative $\partial n_I/\partial r$, that (notwithstanding the uncertainties mentioned above) is known to be positive in both positions at all times indicated in the figure, is clearly much higher at *b* than at *a*. Therefore, if the transport is dominated by diffusion (as it is confirmed by the impurity behaviour during the depletion phase), D(r) has to undergo a very strong reduction over the short distance from *a* to *b* (generally less than 0.25 m). The peaks of the $\Delta\varepsilon_{SXR}$-profiles in that figure are therefore located at the edges of the region of high diffusivity.

The fact that after an initial phase of very rapid propagation the progression of the impurities towards the centre comes practically to a halt confirms the deduction of an abrupt radial change in D(r) as discussed above. The thick lines of fig. 4 (bottom), drawn through the peaks at given times of the $\Delta\varepsilon_{SXR}$-profiles show this clearly. At the first sawtooth collapse (80 msec after Ni injection) Ni ions are suddenly transported towards the centre, as evidenced by the

displacement of the thick lines of fig. 4 (bottom) at 9.58 sec. The central Ni density profile is not completely filled by this event, since $\Delta\varepsilon_{SXR}$ remains hollow as clearly shown in fig. 3 (bottom). Only at the subsequent sawtooth collapse about 80 msec later is the centre filled and does $\Delta\varepsilon_{SXR}$ peak at the centre. At these first two sawteeth the central soft X-ray brightness displays an inverted behaviour, that is it undergoes a sudden increase, instead of a decrease at the sawtooth collapse.

The soft X-ray emissivity is seen to evolve very slowly at all times within the position *b* of fig. 4 (top) both during the ingress phase (i.e. when the $\Delta\varepsilon_{SXR}$ profile is hollow) and during the depletion phase with peaked $\Delta\varepsilon_{SXR}$ profiles. This is the evidence that D is very low over most of that region and not only locally around *b*. There is however always the mentioned exception of the sawtooth collapses. During the depletion phase, contrary to the inverted sawtooth cases of the inflow, the impurity ions are displaced outwards at the crashes, i.e. towards the external high diffusivity region. The central soft X-ray brightnesses abruptly decrease at the crashes displaying the normal sawtooth behaviour. In conclusion, in all cases the sawteeth short-circuit the two regions with different diffusivities.

3. ANALYSIS OF TRANSPORT AND UNCERTAINTIES

Because of the aforementioned difficulties with the determination of the transport parameters with a direct method from the soft X-ray cameras, and in view of the complementarity of information from different signals, the best method of analysis for these experiments remains the check of consistency of simulations of the impurity transport with the relevant diagnostic data. This method is described in detail in Ref. [3]. In Ref. [23] the atomic data used to describe ionisation, recombination and line or continuum emission are discussed.

The impurity flux density is expressed as the sum of a diffusive and a convective term:

$$\Gamma_Z(r) = -D(r)\,\partial n_Z/\partial r - V(r)\,n_Z(r).$$

D(r) and V(r) are radius dependent diffusion coefficient and inward convection velocities - the same for all ionisation states of charge Z and density $n_Z(r)$. Away from the sawtooth crashes, these profiles are kept constant in time throughout

the simulation: an assumption that is justified by the relative steadiness of the discharges and by the short duration of the analysed phenomenon.

Once two regions with distinct transport properties have been localised, as starting point of the simulation D(r) is set to constant values, D_{in} and D_{out} respectively, in each region with a third transition region in-between. D(r) is subsequently adjusted, by modifying the two constant values, smoothing or sharpening the transition and extending or reducing the width of the central region, to reproduce the absolute values of the $\Delta\varepsilon_{SXR}(r,t)$ profiles and the time evolution of the monitored emission lines. Due to the limited spatial resolution of the soft X-ray cameras (~ 10 cm), however, the D(r) functions obtained in this way (illustrated later in fig 7) are to be considered to some extent a schematic description of the real profiles. Local short-wavelength perturbations of these shapes would not substantially impair the agreement with the data, even with amplitudes comparable to the absolute value of D. However the effective value in the outer zone D_{out} is typically accurate within ± 30%. Values of D_{out} outside that range would not allow to reproduce the time evolution of both the ingress and depletion of impurities, for any choice of the velocity profile. The value for the central slow transport region D_{in} suffers from a higher relative uncertainty (± 70%).

The convection profile V(r) is initially assumed to be given by assuming $V(r) = 2\ S\ D(r)\ r/a^2$, with the peaking factor S = 1 everywhere. The V-profile is subsequently adjusted as is done for D(r) in order to reproduce the experimental data. This procedure leads to values of the inward convection velocity lower than or of the order of ~ 0.1 m/s in the inner region of the discharge. Substantially higher values (by a factor of 3 to 4) would imply too high impurity inflows in the centre during the initial phase and would lead to premature and too strong filling of the core with the injected impurities. During that phase, diffusion is dominating and the simulation is generally not very sensitive to the exact shape of V(r) at the transition region and in the inner half of the large diffusivity region. This was not the case for the slowly diffusing H-mode injections reported in [4], where the slowly increasing $\Delta\varepsilon_{SXR}$ peak amplitudes can be controlled by the V(r) function at and just outside the wide transition region. Further information on the convection/diffusion ratio in the centre is also deduced from the decay of $\Delta\varepsilon_{SXR}(r)$ in the core during the depletion phase. However, for S of the order of 1, the sensitivity of this decay to the values of V in the centre is poor and, even in cases when a long quiescent phase between successive sawtooth-crashes is

available for the study of that decay, the uncertainty on the central values of V is ~ 100%. This was the case for Mo injection during a monster-sawtooth reported in Ref. [3].

Simulation of the peripheral line brightnesses is a well-known difficulty in laser blow-off experiments [3,11]. In the simulations the neutral impurity influx $\phi(t)$ at the plasma edge, that is otherwise unknown, is tailored to describe the line brightnesses of the most peripheral ion monitored (e.g. Ni XIII or Ni XVII for Ni injection). As in JET these last typically for 15-20 msec, $\phi(t)$ is also required to evolve on the same time scale. This is difficult to justify as a product of laser ablation at the target and at the present time it is thought to be due to unknown phenomena during the first ionisations and during the rapid ion propagation along the field lines.

However, even this heuristic ansatz is not always sufficient to describe in detail the time behaviour of line emission from intermediate ionisation states such as Ni XX to XXV, the simulation giving often too fast decay times for lines from these ions. This discrepancy is interpreted as the evidence that the quantity S and/or D is substantially different near the separatrix than it is 0.1 m further in, resulting in a peripheral barrier that prevents a too fast outward diffusion of the intermediate charge states from the outer layers of the plasma column: an effect similar, but much less pronounced, to the one previously observed in H-mode discharges with intrinsic [24,25] and injected impurities [2,4]. A detailed analysis on the necessity of this peripheral barrier can be found in Ref. [26]. This edge modification of the transport parameters may require an increase of D in the high diffusivity region of up to 25% to maintain the simulated central $\Delta\varepsilon_{SXR}(r)$ emissivities and the brightnesses of Ni XXVI and Ni XXVII resonance lines in agreement with the experiment.

With the exception of the 7 MA pulses, in all the simulations reported in this paper the inclusion of the peripheral barrier was not necessary; the emissivity profiles $\Delta\varepsilon_{SXR}(r)$ as well as the Ni XXVI and Ni XXVII brightnesses are well simulated in all cases, whereas the decay of the simulated Ni XXV brightness is sometimes too fast.

The soft X-ray profiles $\Delta\varepsilon_{SXR}(r)$ shown in fig. 3 (bottom) clearly exhibit a discontinuity of the impurity transport at the time of sawtooth collapses that cannot be simulated by considering the drop in T_e alone [3]. The modifications of

the ion distribution occurring at the sawtooth collapses over time intervals lasting 100-200 μsec are quite complicated and require both D(r) and V(r) to be increased by orders of magnitude during those intervals. However no single model could be found capable to describe a whole series of consecutive crashes but ad-hoc adjustment for each sawtooth of the transport perturbation proves necessary. Certainly the simple flattening of the impurity distribution within a certain radius [27] does not describe the details of the observed rearrangements: up to the second inverted sawtooth in pulse #22394, for example, the n_I-profile is still clearly hollow and during the depletion phase global expulsion of the injected impurity from the central region is often observed. The latter can be simulated by a centrally enhanced outward V(r) function[28].

It is worthwhile to stress that our heuristic description of these events is based on a one-dimensional (radial) transport model. There are indications, however, that more complicated flows, intrinsically two-dimensional, are responsible for the exchange of particles in the core of the discharge. This could be studied by following during the crash the two-dimensionally resolved ε_{SXR} and electron temperatures [29]. The latter can be obtained in some cases from the one-dimensional space- and time-resolved electron cyclotron emission profiles by exploiting the rotation of the MHD structures in the plasma [29,30]. Line radiation from ions emitting in layers near the soft X-ray inversion radius r_{inv} should also be useful as their brightnesses are affected differently in the case of ion expulsion from the centre or in that of mixing about the inversion surface.

In fig. 5 a few experimental profiles of $\Delta\varepsilon_{SXR}$ (solid lines) from the shot #27394 are shown and compared with the simulated ones (dashed lines), taking $D_{out} = 1.5\ m^2/s$, $D_{in} = 0.1\ m^2/s$, and $S(r) = 1$. The quiescent phase between the two inverted sawteeth (occurring at times $\Delta t = 0.08$ s and $\Delta t = 0.16$ s after the injection) is the most favourable for studying the central transport parameters, since $\Delta\varepsilon_{SXR}(0)$ is sufficiently large and varying, although only slightly, with time. Variations of D_{in} by a factor of 1.5-2, or V(r) in the central region by a factor of 3-4, produce modifications of the simulated $\Delta\varepsilon_{SXR}(0,t)$ marginally consistent with the experimental data, justifying the error bars quoted above.

Concerning the external region, the simulations of $\Delta\varepsilon_{SXR}$ are more sensitive to D_{out}, as stated before, but quite insensitive to the convection velocity The effect of V(r) is best visible in line intensities from Ni XXV-XXVI-XXVII (pictured together with intensities from Ni XVII and Ni XVIII in fig. 6). The S(r) = 1 case is clearly

the best, while the S = 1.5 and S = 0.5 ones set the limit of compatibility with measured data.

Figs. 7 to 9 show D(r) and V(r) curves, for the n_e, P_{tot}, I_p and B_T scans. The n_e-scan (fig. 7) for I_p = 3 MA, B_T = 3.2 T, P_{add} = 4 MW shows clearly the empirical trend (already reported for JET [2]) of improved confinement at higher electron densities. This point will be considered in the next section. The radiation detected by bolometry increases with n_e and at $\langle n_e \rangle \approx 5\ 10^{19}$ m^{-3} the plasma disrupts following the Ni injection when the total Ni radiated power is of the order of 5 MW.

Fig. 8 confirms the regularly observed degradation of particle and energy confinement with the total power for a series of discharges with I_p =3 MA, B_T = 3.2 T. Neither scan (figs. 7 and 8) shows appreciable variation of the low transport region's size. This is not the case for the I_p scanning (B_T = 3.2 T, P_{add} = 4 MW). Fig. 9 shows a clear increase in size of the slow transport region with increasing I_p. To analyse the influence of the toroidal magnetic field on the impurity transport a discharge in the B_T-scan has also been shown in the figure (pulse #27420, I_p = 2 MA, B_T = 1.45 T, P_{add} = 4 MW). The slow transport region's size appears better correlated with the safety factor than with I_p, since it is the same for shots #27420 and 27416 which have the same value of q_a. A more detailed analysis of the q profile dependence of transport will be presented in Section 4.

The study of the influence of the q-profile has been pursued with a few laser blow-off injection experiments into 7 MA deuterium discharges. Ni has been injected both during the current plateau at 7 MA and during the ramp-up and ramp-down phases at 5 MA. The D(r) and V(r) curves obtained are shown in fig. 10. At 7 MA the results of fig. 9 are confirmed, the low transport region's width increases with current. But there is also a dependence (to be discussed in the next Section) on the q-profile, since during the ramp-up and ramp-down phases the q(r) profile is varying. Two observations need to be made about the simulation of these pulses. Firstly the extension of the large D-value region is quite small and it has not been possible to follow the injected Ni decay phase without having recourse to the peripheral barrier with increased V and/or reduced D discussed previously. Secondly at 7 MA the poor quality of the tomographic reconstruction hinders practically any study of the central plasma after the first inverted sawtooth. After that sawtooth the simulation is based only

on line brightnesses with no information on the sawtooth X-ray emissivity discontinuities. Due to this reason the inner parts of the D(r) and V(r) curves are affected by a higher uncertainty and have been presented by dashed lines.

4. ANALYSIS OF DEPENDENCE ON PARAMETERS

Comparing pulses of fig. 7 and 8 that have the same I_p and B_T, it can be seen that $P_{tot}/\langle n_e \rangle$ is a better ordering parameter for the effective value, D_{out}, of the impurity diffusion coefficient in the region outside the transition than either the electron density or the heating power alone. Indeed, for fixed I_p and B_T (i.e. for similar q profiles), this same parameter appears to order the measured impurity containment times τ_I for the whole data set of JET experiments of non recycling impurity injection. For the pulses analysed in such experiments, D_{out} is also in good correlation with the average of the electron temperature gradient $\langle \nabla T_e \rangle$ over the entire fast transport region (no space resolved information on T_i was available on most of these pulses). The relationship between its value and $\langle \nabla T_e \rangle$ is shown in fig. 11. The data shown are consistent with a power law dependence $D_{out} \propto \langle \nabla T_e \rangle^{\gamma}$ with $\gamma = 0.85 \pm 0.2$. The dependence on ∇T_e cannot be distinguished from a dependence on T_e, (or from a dependence on T_i or its gradient), because of the strong correlation of these two parameters (and because of lack of information on the T_i profile). From the comparison of pulses with practically identical T_e profiles and different density it appears that the level of the electron density (or of its gradient) has no appreciable influence on D_{out} [9]. It appears therefore that the empirical trend, usually found in density scans, of confinement improving with density is the result of the inverse n_e-dependence of T_e when the heating power is kept constant more than a real marked dependence of diffusivity on electron density. For the same reason this result is not in contradiction with the positive n_e-dependence of τ_I reported in the past [2] because, as most of the discharges used for that analysis were ohmically heated and all of them were carried out at low total heating power, there was a marked inverse correlation between n_e and T_e.

Above, it was shown that both a reduction of the magnetic field and an increase of the plasma current result in an enlargement of the slow transport region (STR), suggesting the safety factor profile as a crucial factor in determining this feature. In fact varying the total heating power or the average density, while keeping B_T and I_p constant, did not affect its dimension appreciably.

The relationship of the size of the STR and q_a is shown in fig. 12. The diameter of the STR d_{STR} is measured by the distance of the two maxima in $\Delta\varepsilon_{SXR}$ versus the major radius on the horizontal mid-plane 40 ms after the injection (see fig. 4 right). A clear inverse correlation appears from the graph.

An analysis of the D-profile in terms of local parameters, instead of a global one like q_a, is clearly more appropriate, although the experimental uncertainties on the current profile would be expected to make the search difficult. However the abruptness of the transition to high levels of D outside a certain radius suggests to look for a physical parameter that also displays a similarly strong radial variation, and/or that crosses a given critical value, at the same position.

The closeness observed in previous experiments [3] of this position to the locus of sawtooth inversion suggests the equation $q = 1$ as a possible predictor of that position. The profile of q for a $B_T = 3.2$ T, $I_p = 5$ MA discharge is shown in fig. 13. This profile was derived from polarimetric and magnetic probe measurements using the technique described in Ref. [31]. The uncertainty on q is estimated to ±15% in the core of the discharge. On the plot the location of the sawtooth inversion surface from soft X-ray tomography (averaged over two sawteeth before the injection and two "normal" sawteeth after) is also indicated. As discussed in Ref. [32] the measured q profile is consistent with $q = 1$ at the inversion surface. To localise the transition in the diffusivity level, the profiles of $\Delta\varepsilon_{SXR}$, measured during the impurity ingress phase before the inverted sawtooth are also shown on the same figure. The shear $s \equiv (\rho/q)\, dq/d\rho$, is also plotted on the figure. This parameter, that vanishes on the magnetic axis, displays a very fast variation with the radius. It is affected by a larger relative uncertainty than q itself; however, because of its strong relative derivative, the uncertainty on the position where it reaches a given value, e.g. $s = 0.5$, is generally smaller than it is for the safety factor, e.g. $q = 1$. The two positions are practically coincident in the pulse shown in the figure, and close to each other in several cases, but this is, of course, not the general rule.

Fig. 14 summarises the comparison of the $q = 1$ flux surface's diameter on the equatorial plane d_q with d_{STR}. For most cases the value of d_{STR} is within the large uncertainty range for d_q as deduced from the measured q profile, one notable exception being that of a pulse, marked NS in the plot, where the sawtooth (and $m = n$) activity was still absent at the time of Ni injection and only developed more than 1 sec afterwards. In this case the MHD analysis suggests that the $q = 1$

resonance is absent from the discharge and that $d_q = 0$, while the observed d_{STR} is larger than 1 m. The comparison with the estimate of d_q given by the diameter of the soft X-ray inversion surface supplies also a few more cases where this quantity would be too small by some 0.4 m if used as a predictor for d_{STR}. Furthermore it should be pointed out that similar strong depressions in the diffusivity profile extending over sizeable regions in the core of the discharge have also been identified for the intrinsic impurities [33] and for the electrons [5] after pellet injections or during the early phases of the discharge. These are also cases where no $q = 1$ surface is believed to exist anywhere in the discharge. Therefore we must conclude that, although in all the analysed cases the value of q was close to 1 at the radial position where the transition from low to high particle diffusivity occurred, no essential role appears to be played in this transition by the $q = 1$ resonance surface.

A better correlation is found between the low levels of D and low magnetic shear. This relationship is shown in fig. 15. There d_{STR} is plotted versus d_s, the diameter of the flux surface Σ where $s = 0.5$. The error on d_s was estimated using heuristic functional forms for the error on the measured q profile Δq such that the condition $|\Delta q/q|<0.15$ is satisfied (e.g. assuming $\Delta q = 0.3\ q \arctan[k(r+\delta)]/\pi$ and looking for the maximum shifts of Σ while varying the parameters δ and k). The correlation between the two diameters is high and the linear regression ($d_{STR} = (1.02 \pm .18)\ d_s - (.03 \pm .16)$ m) is consistent with the identity of the two quantities $d_{STR} \equiv d_s$. Marginal consistency with this identity would still be obtained adopting the definitions $d_s = d(s=0.35)$ or $d_s = d(s=0.65)$. The data are therefore consistent with s being the critical physical parameter governing the transition from low to high anomalous diffusivity around a threshold value of 0.5 ± 0.15.

The shear s is not the only possible critical parameter that can be deduced from the data. For example, defining d_{sq} as $d(s \cdot q = 0.45 \pm 0.15)$, an equally good correlation between d_{sq} and d_{STR}, as well as statistical consistency of the data with the identity $d_{STR} \equiv d_{sq}$, is found. Threshold conditions on parameters such as $dq/d\rho$ or s/q turn out to be poorer predictors of d_{STR} for any value of the threshold.

The close proximity of the surface Σ with the transition in D appears to be a feature of discharges with sawtooth-affected quasi-steady current profiles as well as of those few where that profile was still evolving during the impurity

injection experiment. The latter class includes the case of a low-ℓ_i current flat top, one case of current ramp-up (I_p = 5 MA, dI_p/dt = 0.5 MA/s, B_T = 3.4 T) and one of I_p and B_T (I_p = 5 MA, dI_p/dt = -0.8 MA/s,$\langle B_T \rangle$ = 3.15 T, $d\langle B_T \rangle/dt$ = -0.25 T/s).

In most sawtooth-affected pulses the region of low diffusivity is also more or less coincident with a region of low temperature gradient, so it could be argued that the observed dependence of D on the shear is only an outward appearance while the essential dependence is on ∇T_e alone or vice versa. However, *a)* the observation that pulses with similar q profiles but different values of T_e (e.g. in the power scans) also exhibit different values of D_{out} and *b)* the existence of cases, as in the monster pulses, where ∇T_e is high but D is low in the core of the discharge indicate that the shear and the temperature gradient (of the ions and/or of the electrons) are both essential and independent parameters in determining the impurity particle diffusivity.

5. COMPARISON WITH THEORETICAL MODELS

In order to answer the question whether the low diffusivities measured in the core of the discharge can be entirely accounted for by neoclassical effects, the neoclassical diffusion D_{neo} was calculated by a computer package [6] from the formulae by Hirshman and Sigmar [34]. The JET geometry was taken into account by performing the proper averages over the flux surfaces calculated from the IDENT-D equilibrium code [31]. This procedure usually yields smaller values than the corresponding circular cross section approximations.

The electron density and temperature profiles were obtained either from Thomson scattering (when available) or from the electron cyclotron emission measurements and far infrared interferometry. Because of the mentioned lack of information on the ion temperature profiles, $T_i = T_e$ was assumed. Only the effects of collisions with the background plasma and the intrinsic impurity were taken into account for the estimate of D_{neo}: a simplification justified because $\alpha \ll 1$. Carbon was assumed to be the main plasma contaminant with such a concentration as to agree with the experimental Z_{eff}.

In general, D_{neo} consists of two contributions, driven by the pressure anisotropy (dominant in the long mean free path limit) and by the poloidal variations of the friction forces respectively. In the core of the analysed discharges, for the

impurities studied in our laser blow-off injection experiments (Z≈25 to 40), their relative magnitudes are comparable.

The calculated D_{neo} in the centre, which can be as low as 0.01 m^2/sec, turns out to be lower than D_{in} by a factor of 2 to 10. Furthermore, while a strong influence of the magnetic field on D_{neo} is predicted by the theory, no such dependencies can be inferred from the experiments: the best determination of D_{in} is never substantially lower than 0.1 m^2/sec or higher than 0.3 m^2/sec. Therefore we have to conclude that a *moderate* anomalous contribution to the impurity particle transport is generally present in the plasma core.

A similarly precise comparison with theoretical predictions of anomalous transport is not possible, because of the wide variety of mechanisms expected to influence the transport of particles, and because of the lack of a complete theory that can supply precise quantitative formulae for the different transport parameters. Even the theoretical studies of specific classes of unstable internal modes suffer from strongly simplifying assumptions on the plasma geometry and composition. Furthermore, they are often limited to a linear analysis of the turbulence and/or a simplified fluid description of the plasma and are generally based on hypotheses about the statistics of the saturated turbulent fields and their effects on the particle trajectories. The predictions so obtained, therefore, are expected to supply only rough approximations for the transport parameters in specific experiments, as recently pointed out by the analysis of Ref. [35]. Consequently, the estimates given for the ion thermal diffusivity, generally based on mixing length arguments, can also be used for the diffusivity of ion test particles (generally not available in the published works) within the same level of approximation. The parametric dependence, however, should be consistent with the observed experimental trends. In particular, any theoretical model for our impurity transport experiments should predict the low anomaly in the diffusion at the plasma centre (found not to be dependent on the details of the density and temperature profiles) as well as the observed dependence of D on the q-profile.

As the anomalous diffusivity in the outer region of the plasma was phenomenologically seen to increase with T_e and/or with its gradient, we shall analyse the relation of our results to the theories based on ion temperature gradient (ITG) driven modes, which predict a positive dependence of diffusion on that parameter. Models based on these modes generally predict too high values for the plasma centre and too low at the edge, as already observed in a recent

systematic analysis of the ion energy transport in JET[36]. Recently however some authors have observed that more detailed analysis of the mode radial structure leads to substantial modifications of the radial dependence of the diffusion coefficients.

In particular Beklemishev and Horton [37] argue that if the turbulence can be described by a collection of radially-localised statistically-independent helical resonant modes (m/n=q), the effective diffusivity should result from the incoherent superposition of the individual modes and would therefore be strongly affected by the density of those resonant modes or excited states. A high density of these states, typical of the regions with high magnetic shear, would result in an enhancement of diffusion with respect to the levels predicted by the local analyses. Vice versa a low density of states, to be found where the shear is low, would produce a reduction with respect to those levels. In order to test this approach against our results, we estimate the ITG diffusivity typical scale by the leading term common to most theoretical works based on a local analysis [36], $D_0 = {}^1/_2 (c_s \rho_s^2/R)$. Here $\rho_s = \rho_i (T_e/T_i)^{1/2}$, ρ_i the gyroradius of the main ions and c_s their sound speed. The quantity D_0 is plotted in fig. 16 for two different pulses: it can be observed that, as mentioned before, its radial trend is opposite to that of the experimental D-profile, represented in the figure by uncertainty bands. The effect of the density of states is accounted for by multiplying D_0 by the appropriate correction coefficient from Ref. [37] $F_{dw} = 3\, k^2 (r^2/\rho_i) (|q'|/\pi^2 q^2)$, with $k = 0.25$. The model D-profiles so obtained appear closely linked in shape to the experimental ones, with consistently low diffusivity in the inner core of the discharge, the low diffusivity zone being wider in the pulse with a wider region of flat q-profile.

A different approach is suggested by Romanelli and Zonca [38]. They assert that toroidal coupling of adjacent modes induces a strong correlation between them, therefore increasing the radial correlation length of the turbulence L_r to a size that for moderate shear ($s = O(1)$) is comparable to the plasma minor radius. This effect strongly enhances the diffusion process at the plasma periphery with respect to previous estimates. In the core of the plasma instead, where a different limit applies ($s \ll 1$), a strong exponential decrease of L_r is predicted

$$L_r \propto L_s \exp(-c/qs),$$

where c is of order unity and L_s is of the size of the plasma minor radius. A mixing length estimate of the diffusion coefficient, $D_R = L_r^2\, c_s/R$, leads to values

of D_R of the order of a few m^2/s, and comparable to our experimental D_{out}, at the radial position r_c where L_r becomes $O(\rho_i/s)$. Here R is the tokamak's major radius. For $r < r_c$, an exponential quenching is predicted for D_R and the effect of turbulence is expected to be reduced drastically. This behaviour is in qualitative agreement with the observations made in our experiments.
Adopting therefore

$$L_r = \rho_i/s$$

as a threshold condition for the transition from slow to fast anomalous transport we obtain

$$sq \approx c/\ln(sL_s/\rho_i).$$

A condition of this kind is not very different from the empirical conditions found consistent with the data described above (e.g. sq = const).

Among the semi-empirical models of anomalous transport, that of Rebut-Lallia-Watkins has been shown to describe many experimental results obtained in a large variety of devices and operation scenarios [39]. A recent extension of this model to include particle transport [40] assumes simple proportionality between the anomalous diffusivities of particles and of thermal energy: $D_{RLW} = \alpha_p \chi_{RLW}$. The authors suggest to assume the same value $\alpha_p = 1/2$ for all the particle species in the plasma including the impurities. This prescription leads naturally, for many cases, to a very strong quench of the anomalous diffusion, or to its complete vanishing, in the centre: a feature similar to the one found in our experiments. This is generally the case in sawtooth affected discharges (see fig. 17 left), where ∇T_e is generally lower, within the mixing radius, than the critical temperature gradient involved in the model. The predicted anomalous diffusion coefficient however is not entirely in quantitative agreement with the experimental profile, although agreement could nearly be recovered by re-scaling the constant α_p. Greater difficulties arise when ∇T_e is large in the centre as in the case of the monster sawtooth shown in fig 17 (bottom). In that case the shape of the diffusion profile is different from the prediction $D_{RLW}(r)$ and a different value of α_p would not reconcile the two profiles.

6. SUMMARY AND CONCLUSIONS

The experiments analysed in this paper confirm previous reports that the diffusion of impurities is much lower in the core of the plasma than it is further out in the discharge. The validity of this result was verified with no exceptions on a set of discharges virtually representative of the whole L-mode parametric domain of JET. However, most of the impurity injection data available refer to conditions close to steady state obtained with central ICRH heating and with gas fuelling of the discharge. Therefore strong correlation exists in the data between, for example, T_e and ∇T_e, n_e and ∇n_e or the local value of the safety factor and its shear. So the specific role of the different local physical parameters in determining the observed transport remains largely uncertain. A marked deterioration in the impurity confinement was observed with increasing values of $P_{tot}/\langle n_e \rangle$ and T_e (and/or ∇T_e) but no clear dependence on n_e could be detected when the T_e-profile was kept constant.

The average value of the particle diffusivity in the region of slow transport is affected by a large relative error as is the estimate of the neoclassical transport parameters. Yet it appears from the data that a moderately anomalous particle diffusion is present in that region whose level is rather insensitive to the local density and temperature or to the intensity of the magnetic field. Although the level of D found in the plasma core is never much higher than 0.2 m^2/sec its ratio to the neoclassical estimate of that parameter can be as high as 10.

The size d_{STR} of the region where the transport is slow was seen to vary between 0.6 and 1.45 m depending upon the values of the plasma current and the toroidal magnetic field but not on the total heating power or the plasma density and temperature profiles. A few cases of pulses where the current profile is evolving indicate that that size can also be affected by ramping the current in time. The shape of the q profile appears a crucial factor in determining d_{STR}: the wider the area where the q profile is flat the larger that diameter is found to be. Local analysis is consistent with the physical ansatz that the transition from low to high anomalous transport is governed by a threshold condition on some critical parameter involving the shear s. In any case there is clearly a strong positive dependence of the anomalous diffusion on that parameter.

Transport modelling based on the critical ∇T_e assumption leads to shapes of D-profiles similar to those found experimentally when the temperature profiles

are flat in the centre. However, it appears difficult to reconcile the experimentally observed radial dependencies of the diffusion profiles with those derived by those models when the temperature profile is peaked in the centre. Our experimental data indicate that the impurity diffusion in the centre of the plasma, where the shear is low, is very small also when the electron temperature gradient is high. Strong positive dependencies of anomalous diffusion on the magnetic shear have been recently suggested by authors who have initiated the analysis of the radial structure of microturbulent fluctuations inside the discharge. The two theoretical works discussed above are clearly far from supplying a consistent complete theory of ITG-driven anomalous transport and indeed represent complementary and partly contradictory approaches. They both indicate effects leading to the enhancement of transport where the density of resonant modes is high and to its reduction in the low shear regions. This appears in agreement with our observations, although a thorough quantitative comparison is far from feasible at this stage.

ACKNOWLEDGMENT

The authors wish to acknowledge the encouragement and continuing support to this work they received from L. Laurent and P. Thomas. Useful discussions with F. Romanelli are also gratefully acknowledged.

REFERENCES

[1] SHIMADA M., Fusion Engineering and Design **15** (1992) 325

[2] HAWKES N., WANG Z., BARNSLEY R. et al., in Controlled Fusion and Plasma Physics (Proc. 16th Eur. Conf. Venice, 1989), Vol 13B, Part I, European Physical Society (1989) 79.

[3] PASINI D., MATTIOLI M., EDWARDS A.W., et al. Nucl. Fusion **30** (1990) 2049.

[4] PASINI D., GIANNELLA R., LAURO TARONI L. et al., Plasma Phys. Controll. Fusion **34** (1992) 677.

[5] GIANNELLA R., HAWKES N., LAURO TARONI L., et al. Plasma Phys. Controll. Fusion **34** (1992) 687.

[6] LAURO-TARONI L., GIANNELLA R., in Controlled Fusion and Plasma Physics (Proc. 1992 Int. Conf. Innsbruck) Vol. 16C, Part I, European Physical Society (1992) 287.

[7] CHEETHAM A. D., GONDHALEKAR A., DE HAAS J. C. et al., in Plasma Physics and Controlled Nuclear Fusion Research 1988 (Proc. 12th Int. Conf. Nice 1988), Vol 1, IAEA, Vienna (1989) 483.

[8] O'ROURKE J., GOWERS C., KRAMER G. et al., Plasma Physics and Controlled Nuclear Fusion **35** (1993) 585.

[9] PASINI D., GIANNELLA R., LAURO-TARONI L., MAGYAR G., MATTIOLI M., in Controlled Fusion and Plasma Physics (Proc. 1992 Int. Conf. Innsbruck) Vol. 16C, Part I, European Physical Society (1992) 283.

[10] GIANNELLA R, DENNE-HINNOV B., LAURO-TARONI L., MAGYAR G., MATTIOLI M., in Controlled Fusion and Plasma Physics (Proc. 20th Eur. Conf. Lisbon, 1993), Vol 17C, Part I, European Physical Society (1993) 43.

[11] STRATTON B. C., FONCK R. J., HULSE R. et al., Nucl. Fusion **29** (1989) 437.

[12] MARMAR E. S., RICE J. E., TERRY J., SEGUIN F., Nucl. Fusion **22** (1982) 1567.

[13] MAGYAR G., BARNES M. R., COHEN S., et al. JET Report JET-R(88)15.

[14] RUTHERFORD P., HIRSHMAN S., JENSEN., et al. in Plasma-Wall Interactions (Proc. Int. Symp. Julich 1976) Pergamon Press,New-York (1977) 173.

[15] O'ROURKE J., Plasma Phys. Controll. Fusion **33** (1991) 289.

[16] FONCK R.J., RAMSEY A.T., YELLE R.V., Applied Optics **21** (1982) 2115.

[17] SCHWOB J.L., WOUTERS A.W., SUCKEWER S., FINKENTHAL M., Rev. Sci. Instrum. **38** (1987) 1601.

[18] BARTIROMO R., BOMBARDA F., GIANNELLA R. et al., Rev. Sci. Instrum. **60** (1989) 237.

[19] MAST K.F., KRAUSE H., BEHRINGER K. et al., Rev. Sci. Instrum. **56** (1985) 969.

[20] EDWARDS A.W., FAHRBACH H.U., GILL R.D. et al., Rev. Sci. Instrum. **57** (1986) 2142.

[21] WEISEN H., PASINI D., WELLER A., EDWARDS A. W., Rev. Sci. Insrum. **62** (1991)1531.

[22] THE JET TEAM, in Plasma Physics and Controlled Nuclear Fusion Research 1990 (Proc. 13th Int. Conf. Washington, DC, 1990) Vol. 1, IAEA, Vienna (1991) 27.

[23] MATTIOLI M., DEMICHELIS C., MONIER-GARBET P. et al., Cadarache Report EUR-CEA-FC 1491 (1993).

[24] GIANNELLA R., BEHRINGER K., DENNE B. et al., in Controlled Fusion and Plasma Physics (Proc. 16th Eur. Conf. Venice, 1989), Vol 13B, Part I, European Physical Society (1989) 209.

[25] GIANNELLA R., LAURO-TARONI L., BARNSLEY R., et al. in Controlled Fusion and Plasma Physics (Proc. 17th Eur. Conf. Amsterdam, 1990), Vol 14B, Part I, European Physical Society (1990) 247.

[26] DENNE-HINNOV B., GIANNELLA R., LAURO-TARONI L., et al in Controlled Fusion and Plasma Physics (Proc. 20th Eur. Conf. Lisbon, 1993), Vol 17C, Part I, European Physical Society (1993) 55.

[27] PETRASSO R., SEGUIN F., LOTER N., et al. Phys. Rev. Lett.**49** (1982) 1826.

[28] TFR GROUP, Nucl. Fusion **25** (1985) 981.

[29] NAGAYAMA Y., McGUIRE K., BITTER M., et al. Phys. Rev. Lett. **67** (1991) 3527.

[30] CAMPBELL D.J., EDWARDS A.W., PEARSON D., in Controlled Fusion and Plasma Physics (Proc. 16th Eur. Conf. Venice, 1989), Vol 13B, Part II, European Physical Society (1989) 509.

[31] BLUM J., LAZZARO E., O'ROURKE J., KEEGAN B., STEPHAN Y., Nucl. Fus. **30** (1990) 1475.

[32] WOLF R.C., O'ROURKE J., EDWARDS A.W., VON HELLERMANN M., Nucl. Fus. **33** (1993) 663.

[33] BEHRINGER K., DENNE B., GOTTARDI N., VON HELLERMANN M., PASINI D., in Pellet Injection And Toroidal Confinement IAEA-TECDOC-534, Vienna, 1989, p. 167.

[34] HIRSHMAN S.P., SIGMAR D.J., Nucl. Fus. **21** (1981) 1079.

[35] SYNAKOWSKI E.J., EFTHIMION P.C., REWOLDT G., et al. Phys. Fluids **B5** (1993) 2215.

[36] CONNOR J.W., MADDISON G.P., WILSON H.R., et al. Plasma Phys. Controll. Fusion **35** (1993) 319.

[37] BEKLEMISHEV A.D., HORTON W., Phys. Fluids **B4** (1992) 200.

[38] ROMANELLI F., ZONCA F., in Controlled Fusion and Plasma Physics (Proc. 20th Eur. Conf. Lisbon, 1993), Vol 17C, Part IV, European Physical Society (1993) 1387.

[39] REBUT P.H., WATKINS M.L., GAMBIER D.J., BOUCHER D., Phys. Fluids B3 (1991) 2209.

[40] BOUCHER D., REBUT P.H., WATKINS M., C. R. Acad. Sci. Paris, **315 II** (1992) 273.

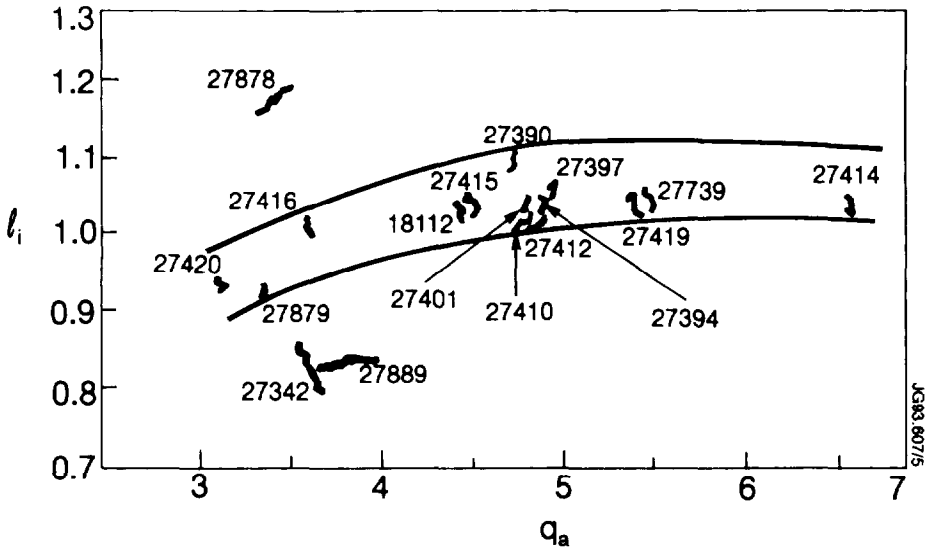

Fig. 1. Trajectories in the q_a- ℓ_i plane during a period of 1 sec starting 0.5 sec before the impurity injection for the discharges analysed in this paper.

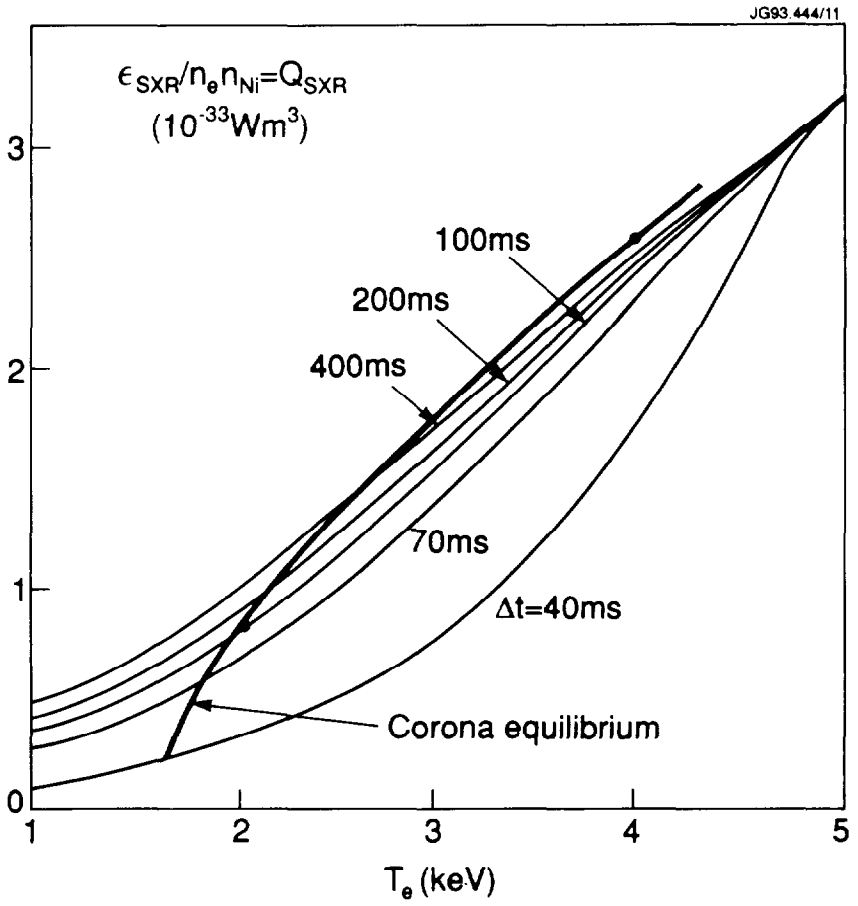

Fig. 2. Effective rate coefficient Q_{SXR} for emission of radiation by nickel as obtained in the transport simulation at different times Δt after the impurity injection. The thick solid line gives Q_{SXR} at corona ionisation equilibrium.

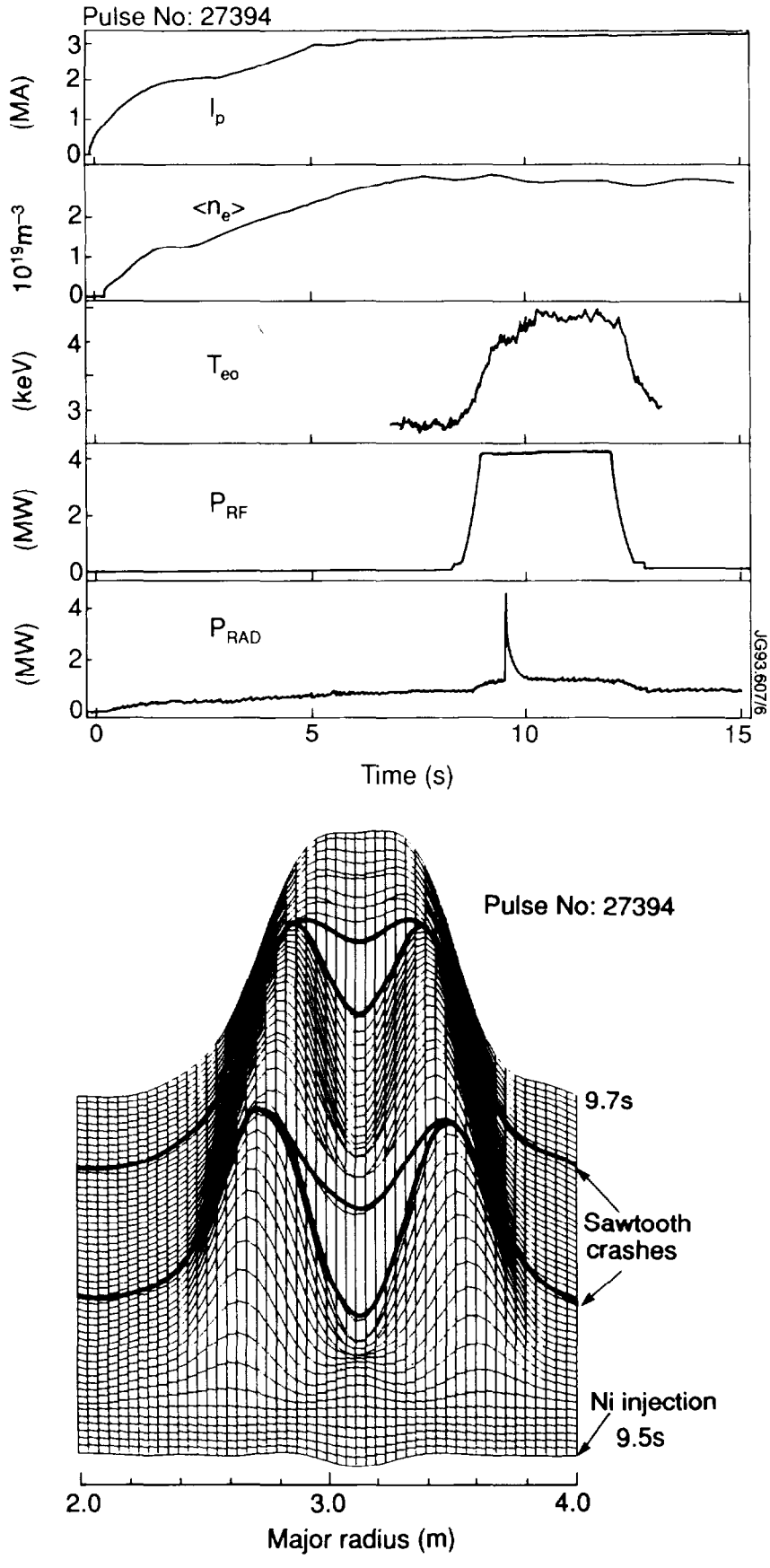

Fig. 3. Time evolution of plasma current, average electron density, peak electron temperature, RF heating power, and total radiated power in an L-mode discharge where injection of Ni by laser blow-off was performed (top). Tomographically inverted soft X-ray emissivity perturbation $\Delta\varepsilon_{SXR}$ along a horizontal radial chord through the magnetic axis as a function of time following the injection (bottom).

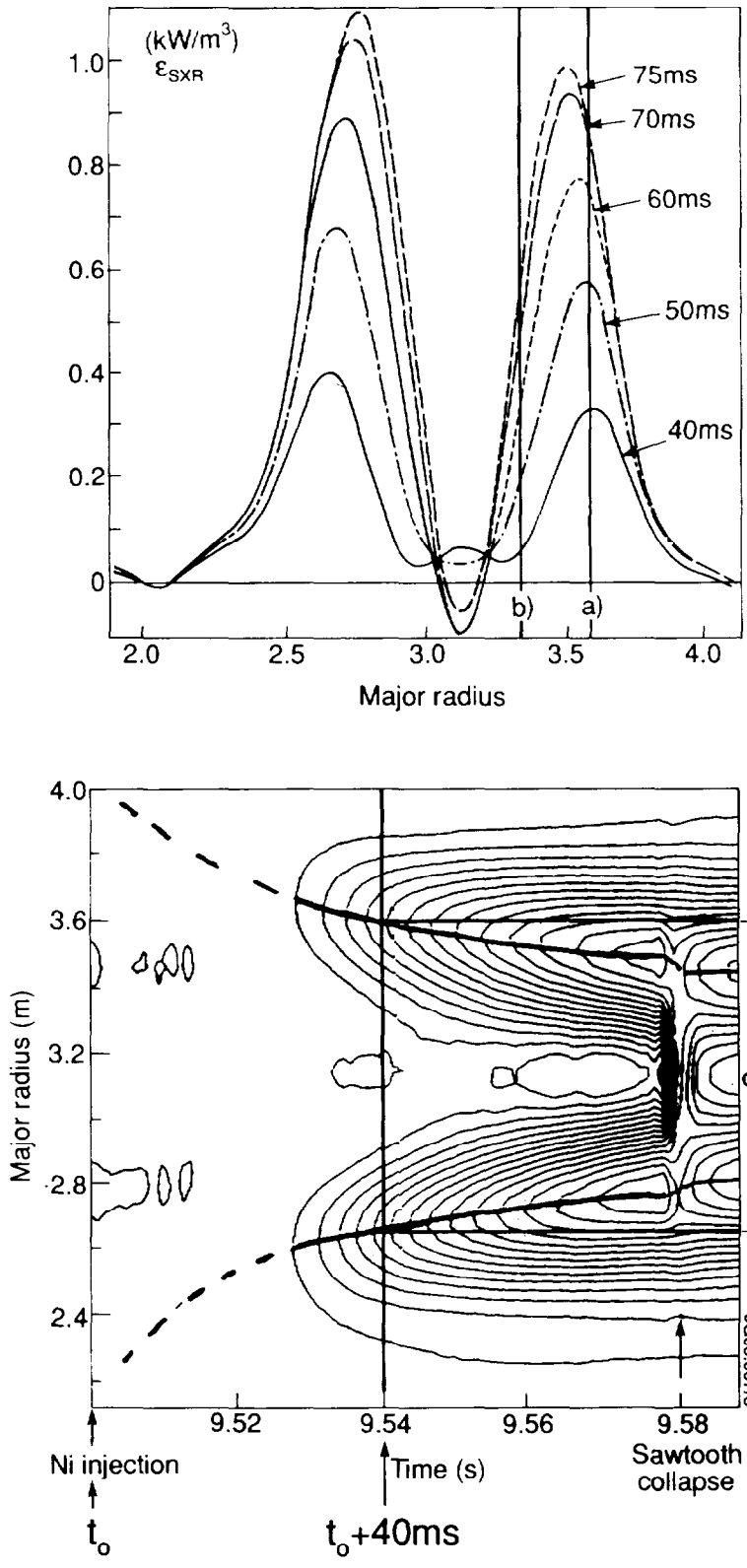

Fig. 4. Profiles of $\Delta\varepsilon_{SXR}$ along a horizontal radial chord at different times Δt after the injection of Ni into the discharge (top). Contours of constant $\Delta\varepsilon_{SXR}$ in the *major radius-time* plane. The thick lines describe the trajectory of maxima in the profiles (bottom). JET pulse #27394.

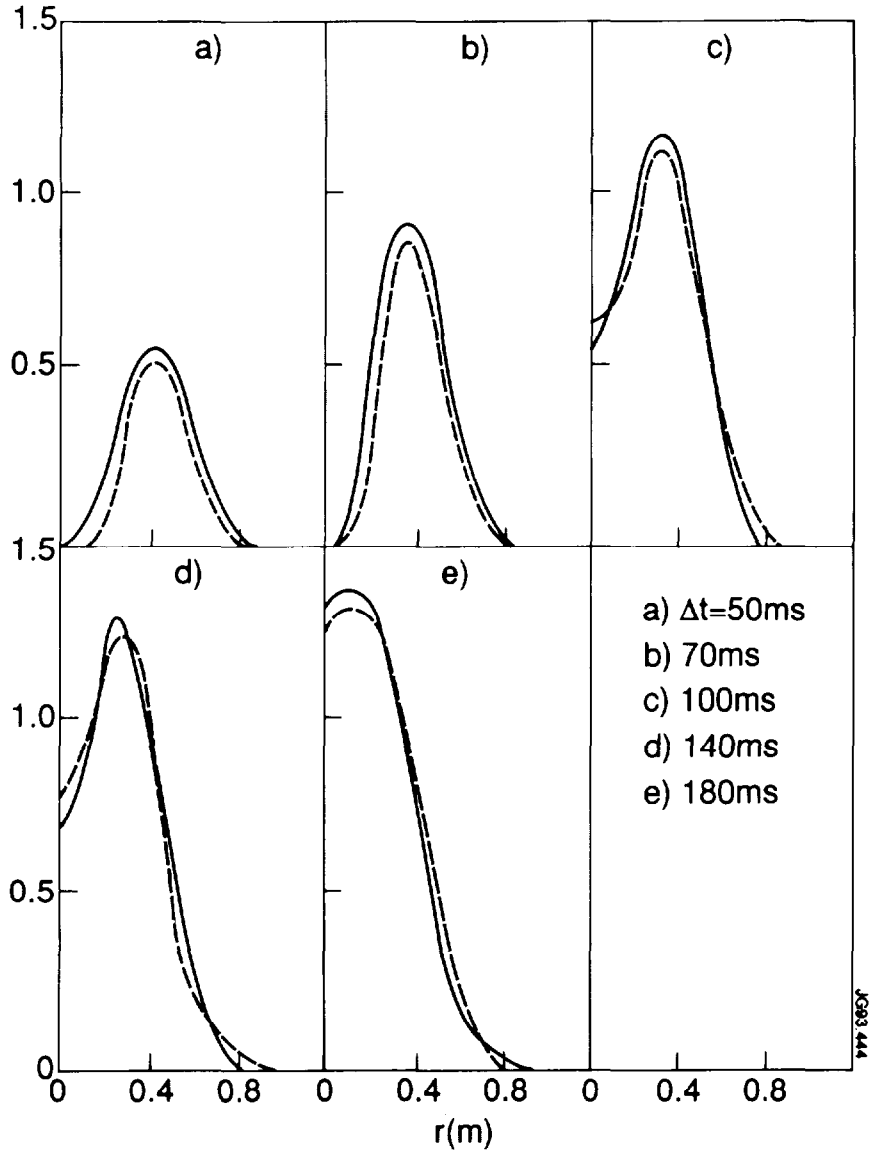

Fig. 5. Experimental (solid lines) and simulated profiles (dashed lines) of the emissivity perturbation $\Delta\varepsilon_{SXR}$ between times $\Delta t = 50$ ms and $\Delta t = 180$ ms after injection of nickel in JET pulse #27394. $D_{out} = 1.5$ m^2/s, $D_{in} = 0.1$ m^2/s, and $S(r) = 1$ is assumed for the simulation.

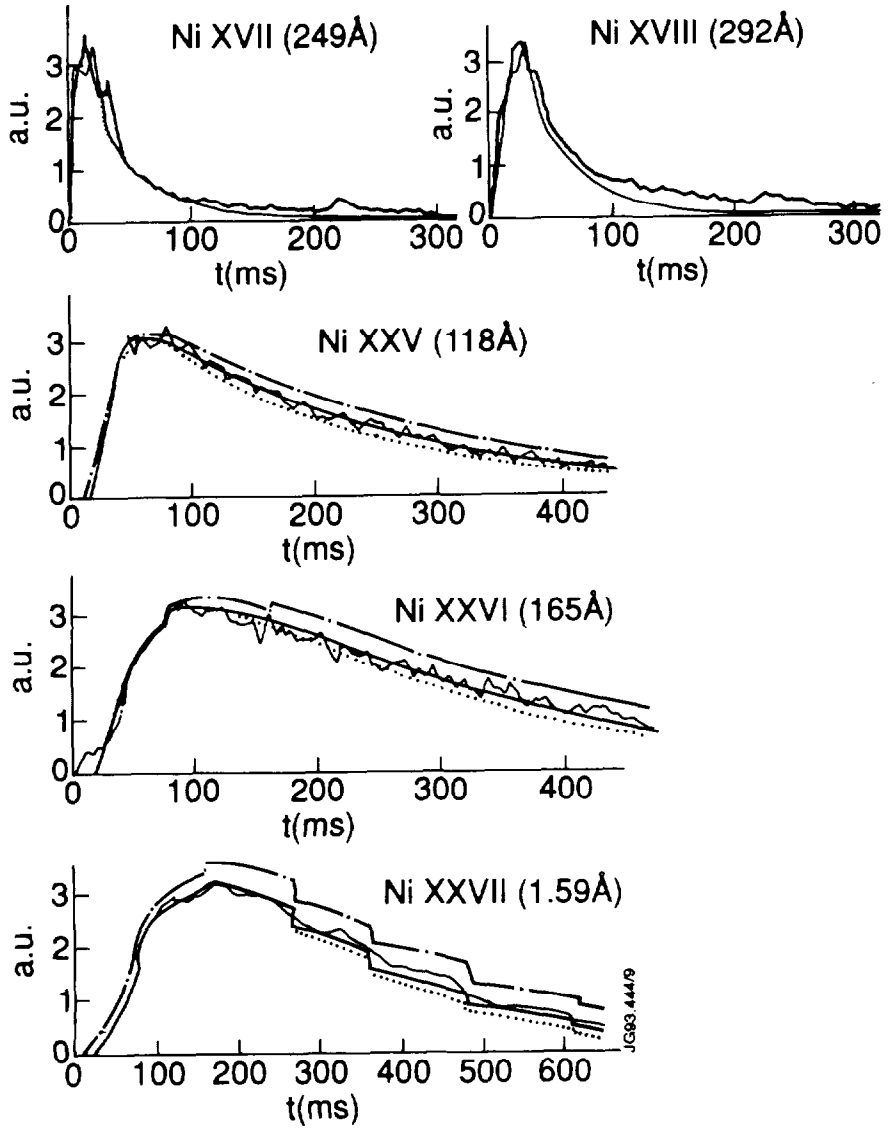

Fig. 6. Time evolution of experimental line intensities from different Ni ion states following injection of nickel in JET pulse #27394. Also shown are the simulated intensities obtained when S = 0.5 (dotted line), S = 1 (solid line) or S = 1.5 (dash-dotted line) is assumed in the simulation.

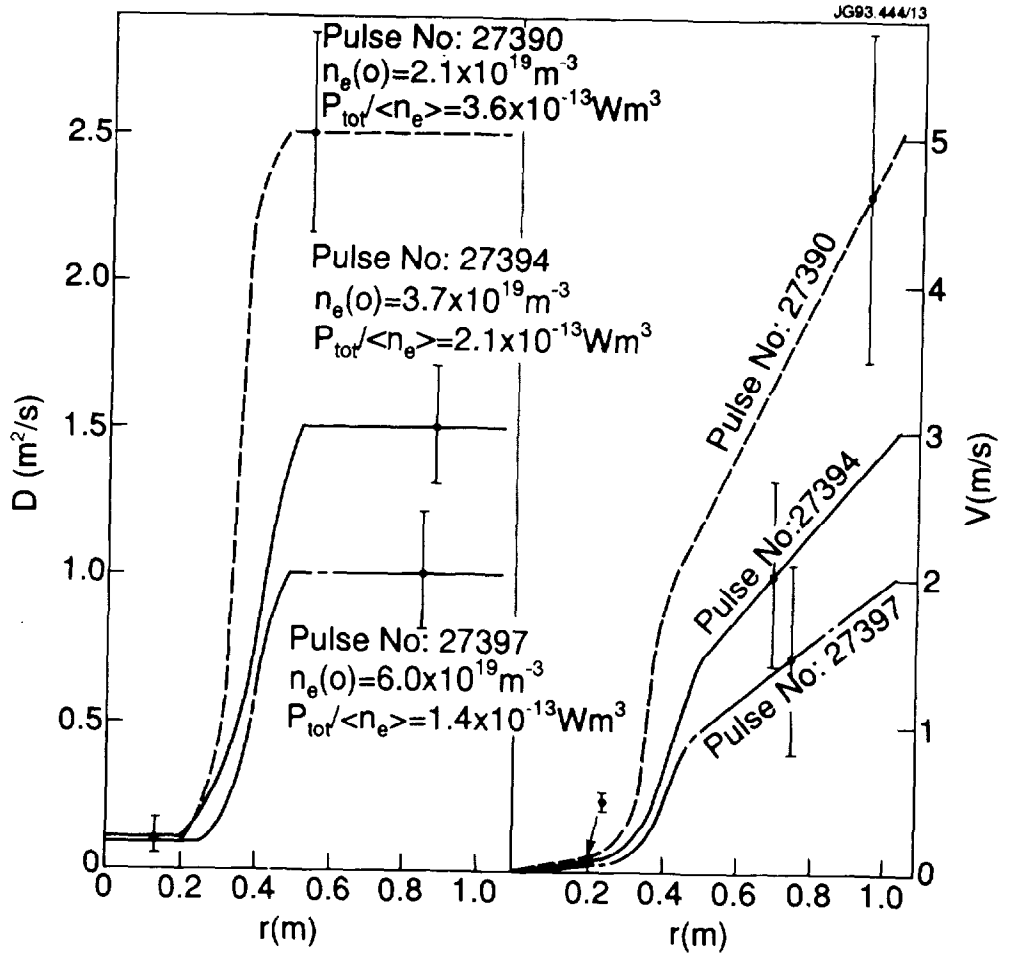

Fig. 7. D(r) and V(r) for ^{4}He plasma pulses from the n_e-scan. For these pulses I_p = 3 MA, B_T = 3.2 T, P_{add} = 4 MW.

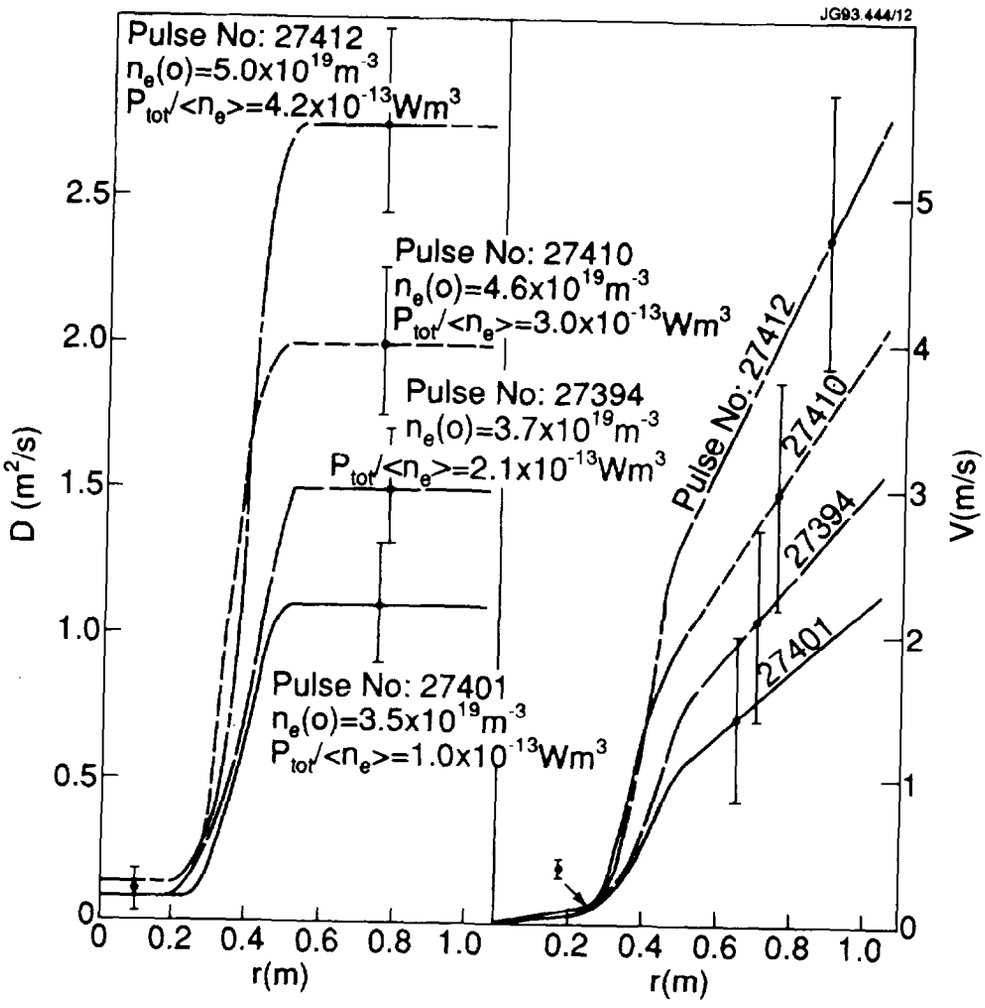

Fig. 8. D(r) and V(r) for ^{4}He plasma pulses from the power scan. For these pulses I_p = 3 MA, B_T = 3.2 T, and P_{add} = 0 to 20 MW.

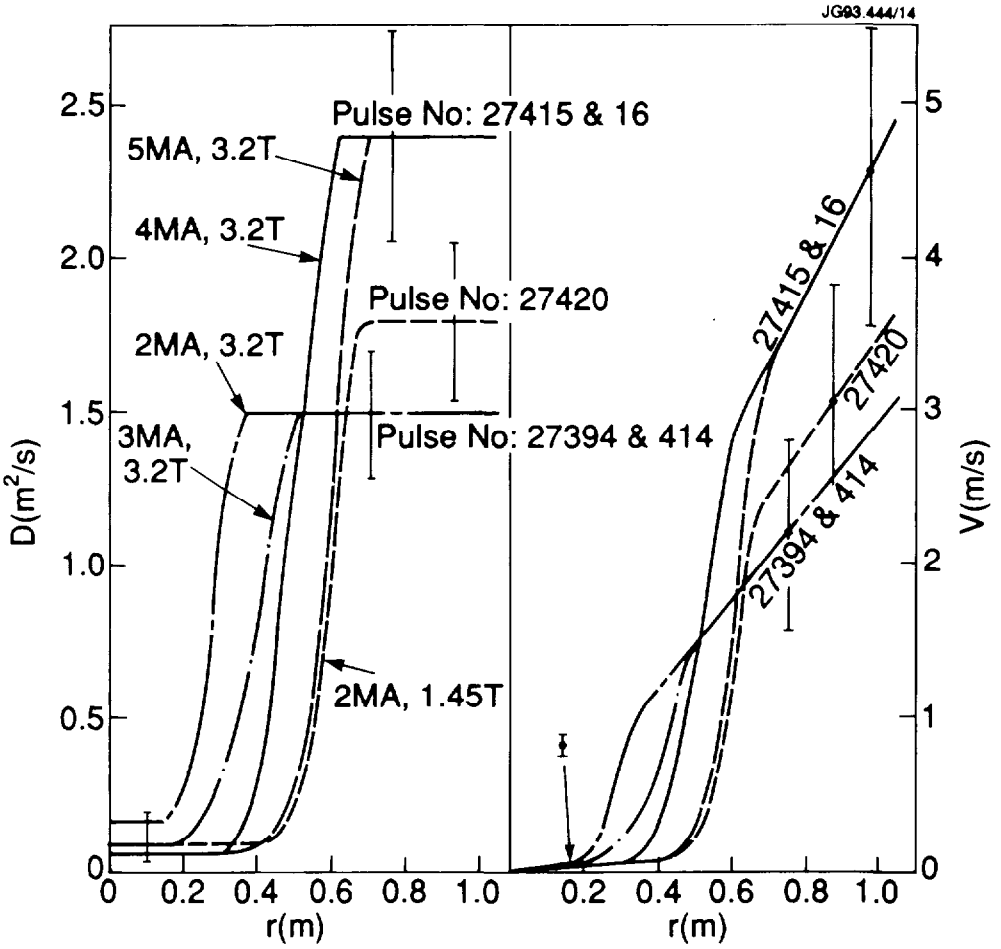

Fig. 9. D(r) and V(r) for ^{4}He plasma pulses from the I_p- and B_T-scan. For these pulses the peak electron density was $n_e(0)$ = 4.2 to 4.8 10^{19} m^{-3} and P_{add} = 4 to 5.5 MW.

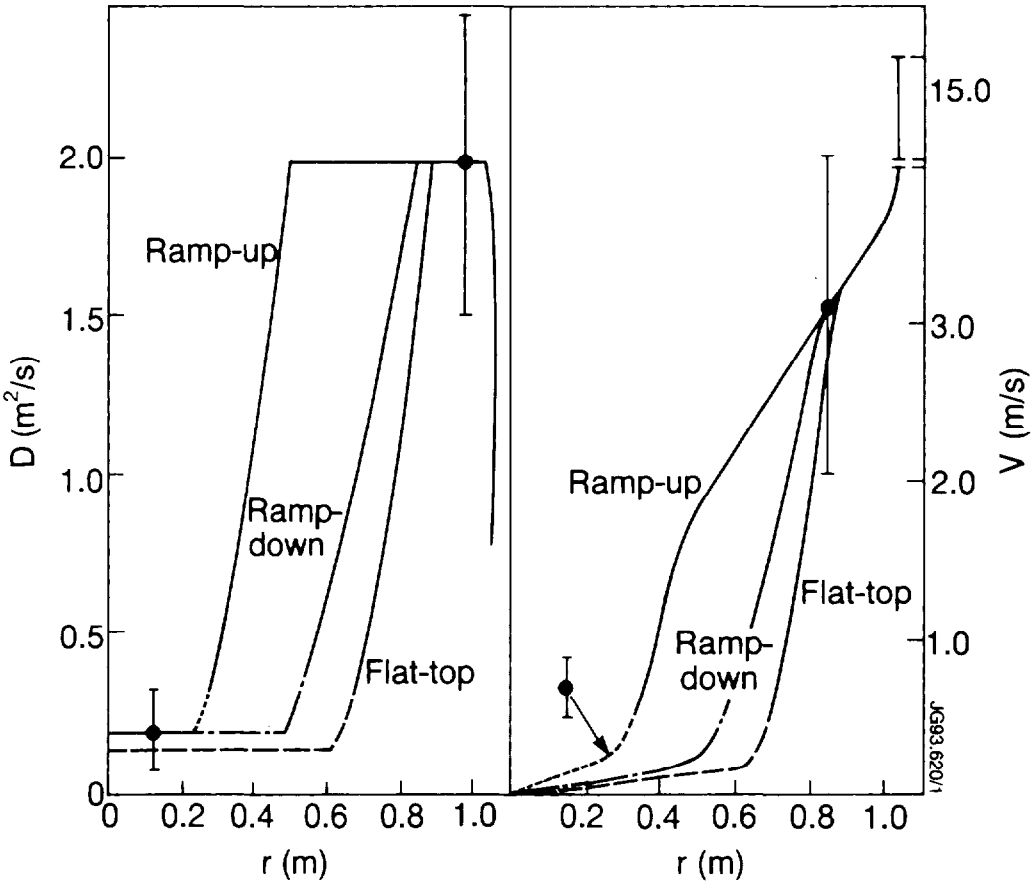

Fig. 10. D(r) and V(r) for 7 MA deuterium plasma pulses. Ni has been injected both during the current plateau at 7 MA, 3.4 T and during the ramp-up (dI_p/dt = 0.5 MA/s, B_T = 3.4 T) and ramp-down (dI_p/dt = -0.8 MA/s, $\langle B_T \rangle$ = 3.15 T, $d\langle B_T \rangle/dt$ = -0.25 T/s) phases at 5 MA.

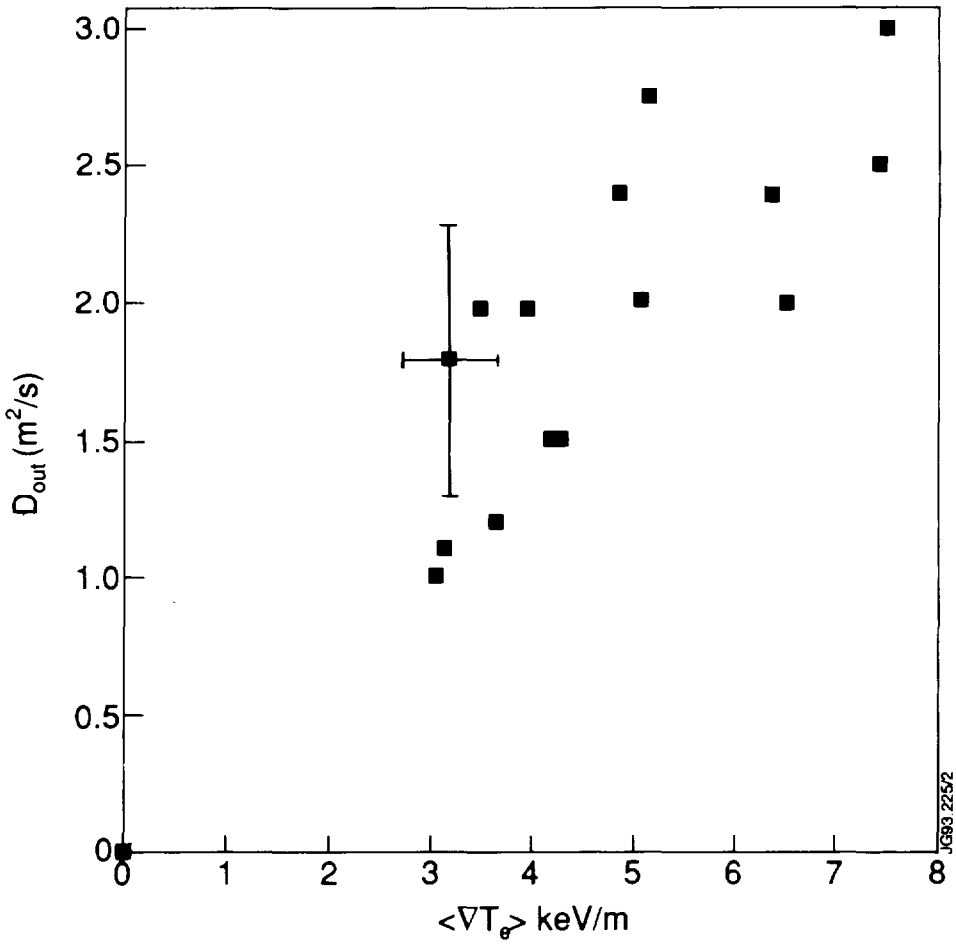

Fig. 11. Average level of the impurity diffusion coefficient in the external fast transport region versus the average over the same region of the electron temperature gradient for L-mode limiter discharges.

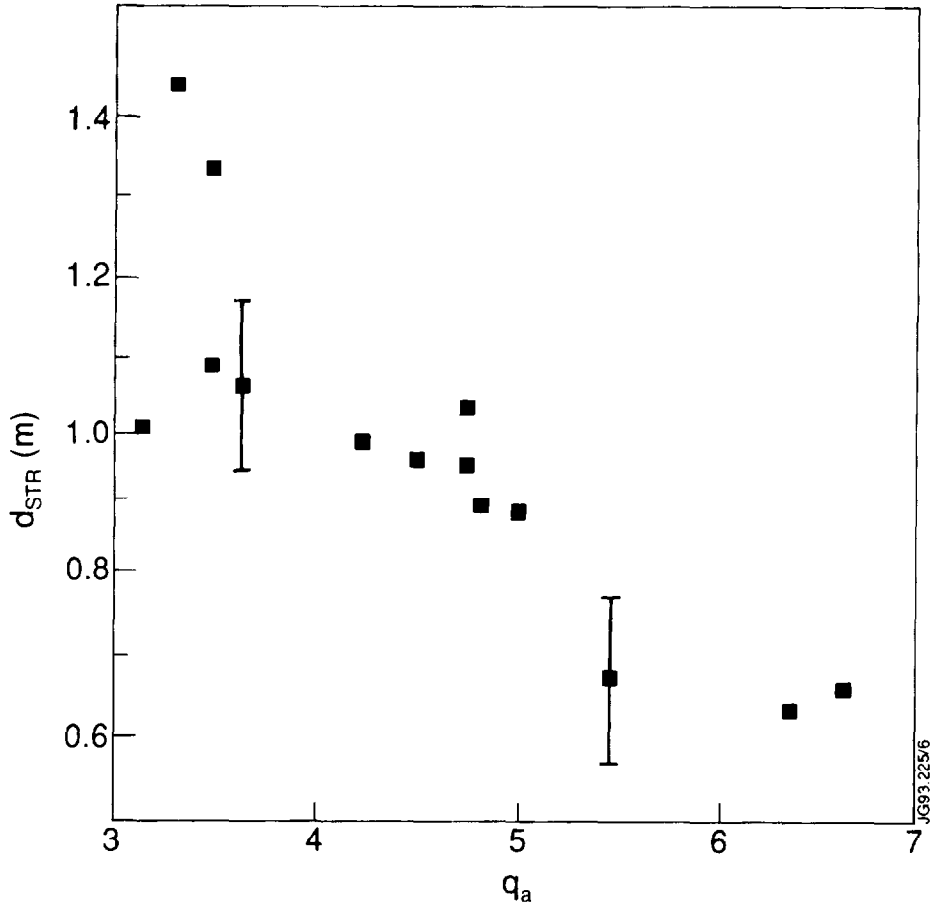

Fig. 12. Horizontal diameter d_{STR} of the slow transport region versus the edge value of the safety factor for L-mode limiter discharges.

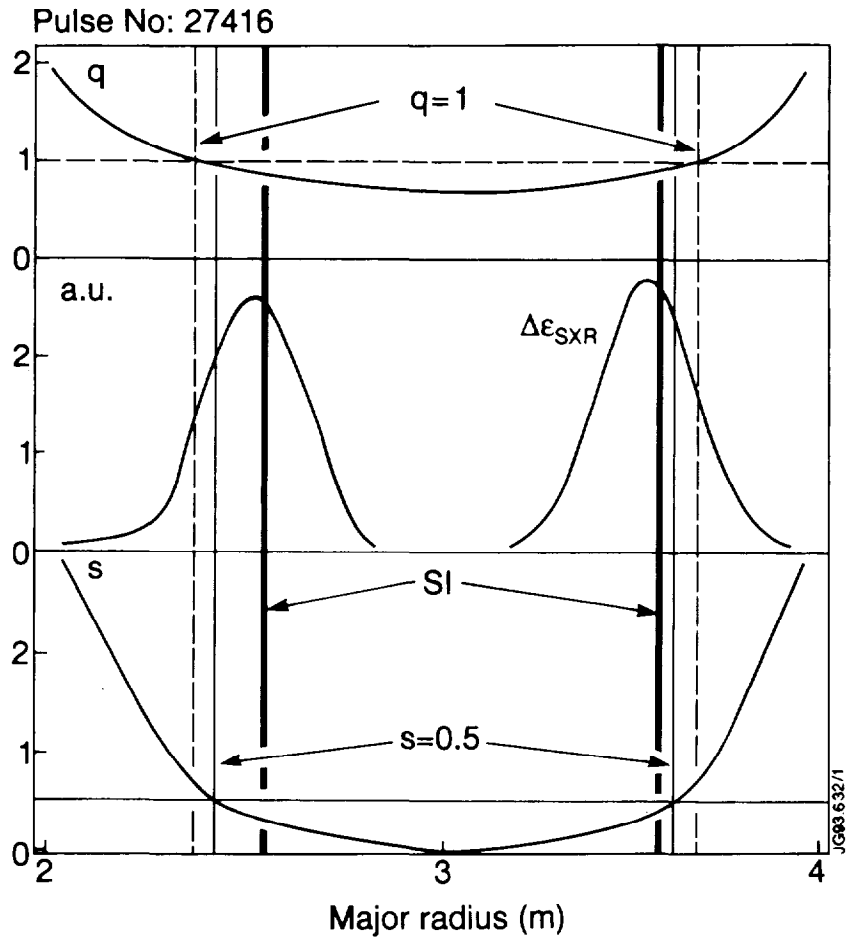

Fig. 13. Safety factor q and shear s for a $B_T = 3.2$ T, $I_p = 5$ MA discharge together with $\Delta\varepsilon_{SXR}$ measured during the impurity ingress phase just before the inverted sawtooth. The surfaces defined by q = 1, s = 0.5 and by the sawtooth inversion (SI) are localised on the diagram by vertical lines.

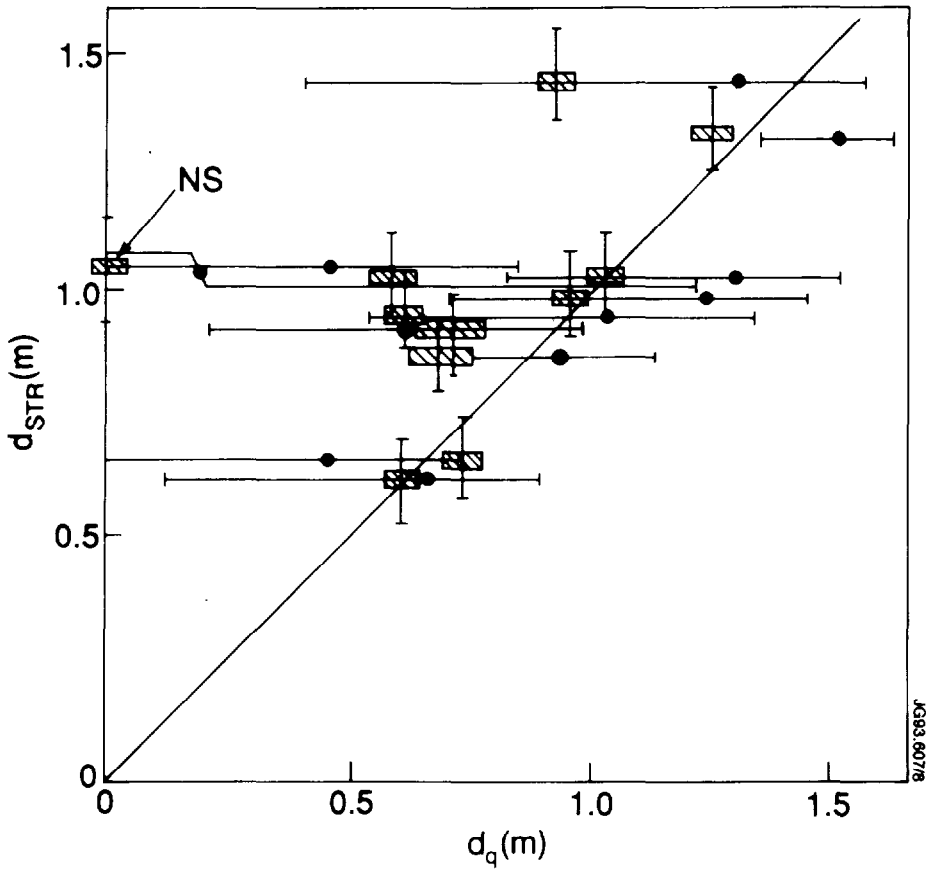

Fig. 14. Horizontal diameter d_{STR} of the slow transport region versus the horizontal diameter d_q of the flux surface where $q = 1$ for L-mode limiter discharges. The filled points show the values of d_q as determined from polarimetric and magnetic probe measurements. For the boxes the diameter of the sawtooth inversion surface was used as determination of d_q. The data point marked NS refers to a pulse where no m=n activity could be detected and the sawtooth activity started only 1 sec after the time of injection. The diagonal straight line represents the identity $d_{STR} = d_q$.

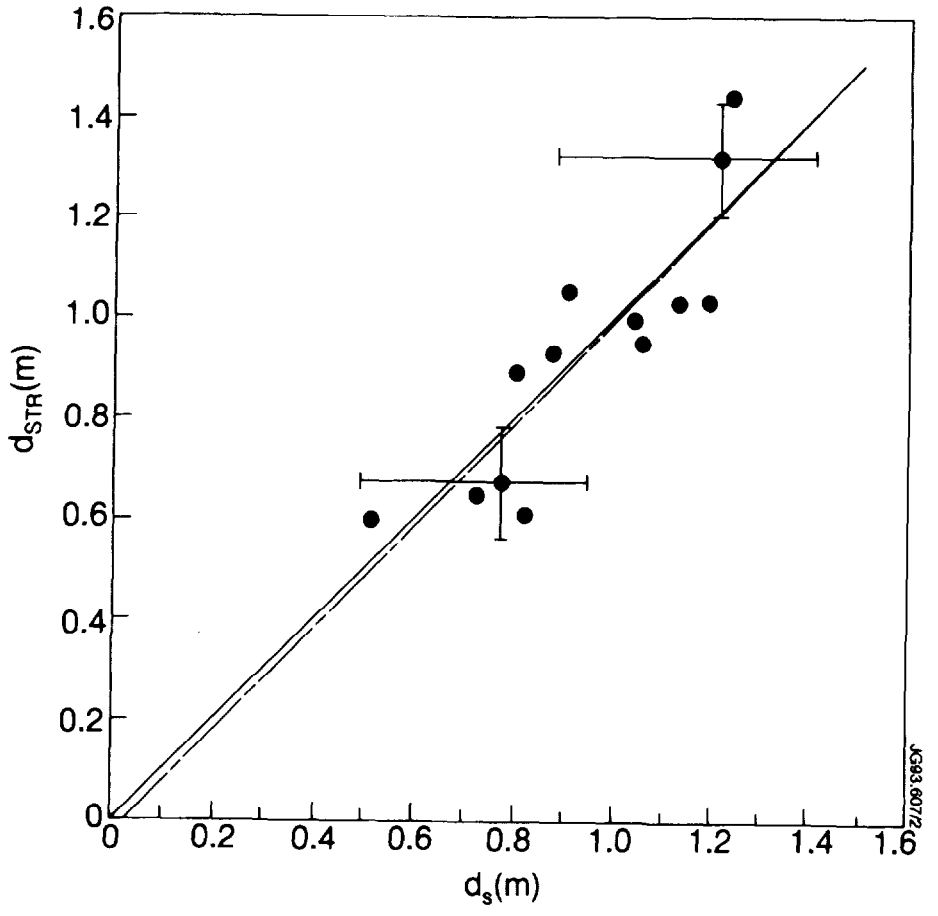

Fig. 15. Horizontal diameter d_{STR} of the slow transport region versus the horizontal diameter d_s of the flux surface where $s = 0.5$ for L-mode limiter discharges. The solid straight line represents the identity $d_{STR} = d_s$, the dashed one the best fit linear regression.

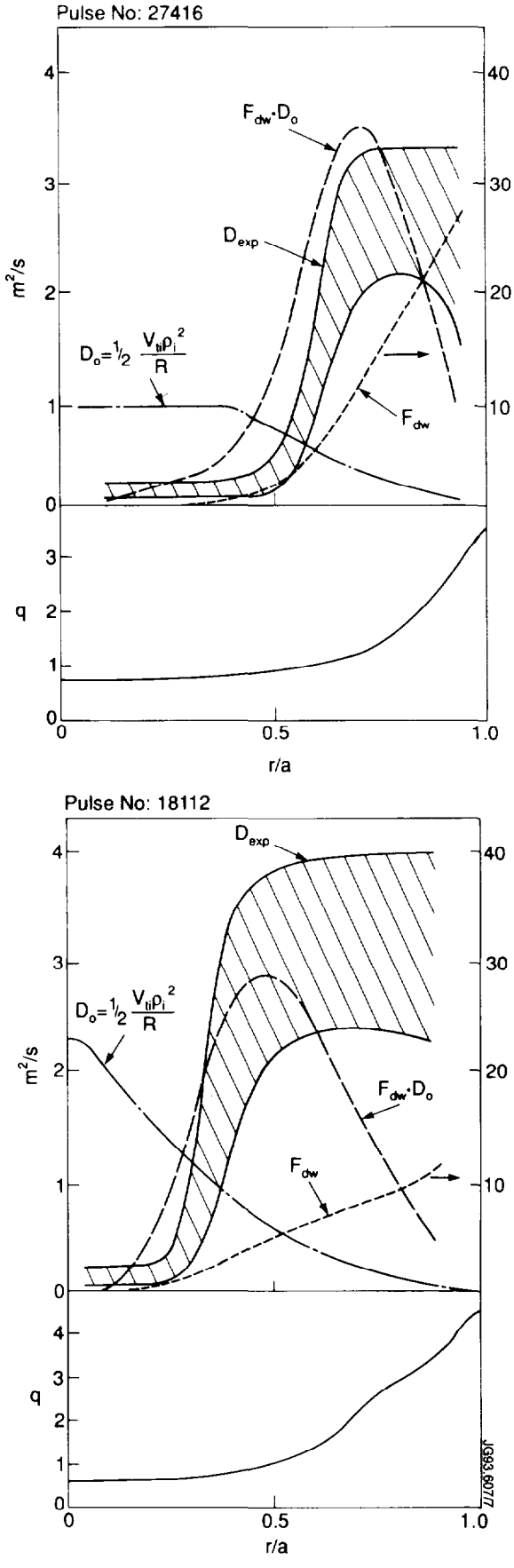

Fig. 16. Experimental profile of the diffusion coefficient D_{exp} for injected Ni in a 5 MA, 3.2 T, P_{add} = 4 MW, ^{4}He discharge (top) and for injected Mo in a 3 MA, 3.2 T, P_{add} = 6 MW deuterium discharge (bottom). Also shown are the typical scale D_0 of ITG turbulence induced diffusivity, the correction coefficient F_{dw} according to Ref. [37] and the product $F_{dw}D_0$. At the bottom of the figure the q profiles are drawn.

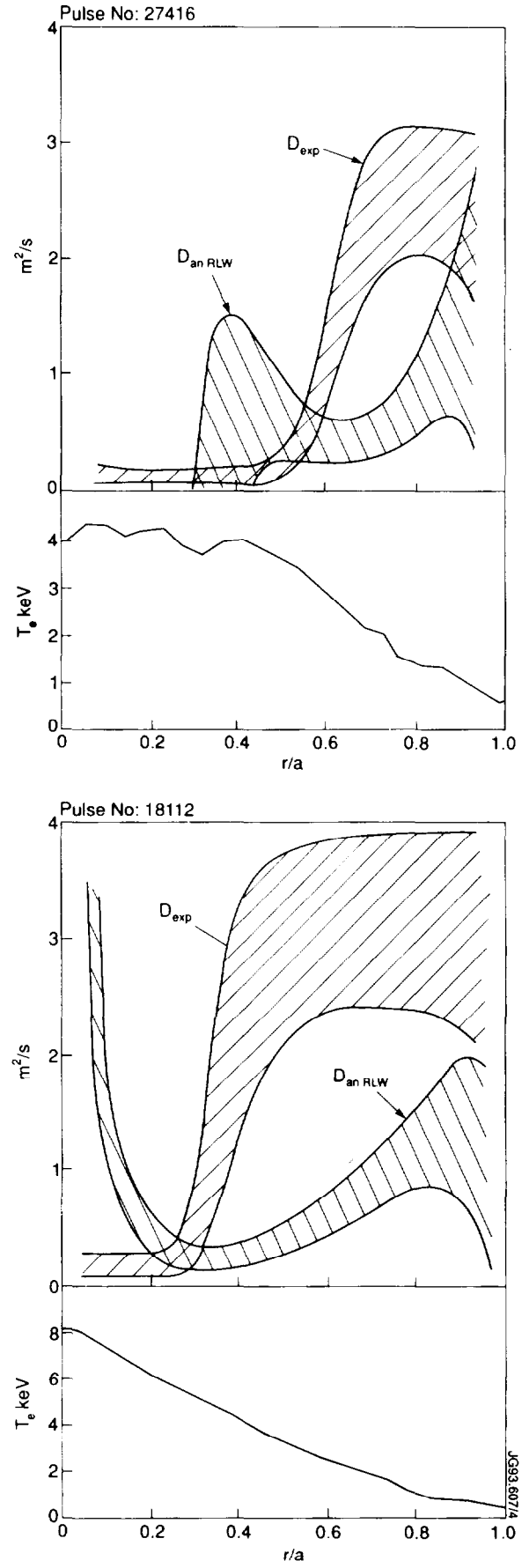

Fig. 17. Experimental profile of the diffusion coefficient D_{exp} for injected Ni in the same two discharges as in fig. 16. Also shown are the profiles of the anomalous particle diffusion coefficient according to Ref. [40]. At the bottom of the figure the T_e profiles are drawn.